

Lumped impulses, discrete displacements and a moving load analysis

A.W.M. Kok

Delft University of Technology, Faculty of Civil Engineering,
Stevinweg 2, 2628 CN Delft, Netherlands

Finite element models are usually presented as relations between lumped forces and discrete displacements. Mostly finite element models are found by the elaboration of the method of the virtual work – which is a special case of the Galerkin’s variational principle –. By application of Galerkin’s variational principle to time dependent problems, considering elements bordered by geometry and time boundaries, we obtain relations between lumped impulses and discrete displacements.

The analogy with respect to static models which formulates relations between lumped forces and discrete displacements is striking. Models are formulated using linear and quadratic displacement fields with respect to time. Free model parameters are used to manipulate numerical stability, accuracy and numerical damping.

These numerical tools are used for the numerical simulation of a moving vehicle at a rail track structure. The analysis shows the natural way of modelling a moving structure (the train) with respect to a fixed supporting structure (the rail track).

Key words: Direct integration methods, finite element models, impulses, nonlinear dynamics, rail wheel interaction, moving loads.

Introduction

Together with the development of the finite element methods much attention has been paid to the development of procedures for the evaluation of transient dynamic analysis problems. The formulation of these models took place along two different paths; the modeling of the geometry followed the procedures of the finite element methods, the modeling with respect to time was an almost pure mathematical procedure. It is seldom attempted to integrate these two processes into one procedure.

Most of the known integration schemes are presented either as a single step algorithm or as a multi-step recurrence scheme. The single step algorithms usually assume continuity of displacements, velocities and accelerations. These processes are easy to interrupt and to restart. The multistep recurrence schemes are slightly more efficient but they don’t have the flexibility of the single step algorithms. A most serious problem is that continuity of velocities and accelerations is not based upon physical requests; in fact discontinuities are, in a physical way, possible. Models that require this continuity may show some shortcomings.

The introduction of time dependency in structural mechanics requires some generalizations. To begin with, a finite element consideration assumes a domain limited by geometry and time. Within this domain we have to formulate the conditions. Secondly the mechanical quantities have to be generalized. The generalization with respect to time introduces impulses in addition to the forces and adds velocities to the kinematic conditions. Instead of the equilibrium conditions for forces we require an impulse balance formulated by the equations of motion. In the static case these equations will degenerate into the equilibrium conditions. The constitutive equations have to include relations between the impulses and the velocities, whereas the stress/strain relations can be time dependent. Finally, the boundary conditions have to be based upon conditions with respect to the impulse balance.

All these conditions together are called the "strong form". The f.e.m. models based upon these considerations will formulate relations between lumped impulses and discrete displacements associated with points located in a finite domain limited by space and time.

The model technique to consider discretisation both to time and geometry in the same step has been applied to model a vehicle moving on a rail track. Because the vehicles degrees of freedom (d.o.f's) are moving with respect to the track d.o.f's the resulting equations are no more symmetric. Because of the large variation of the stiffness properties between the structural components the model may show local overshoot of some results; local adjustment of the free parameters solves this problem completely.

Strong form

Equations of motion:

The basic law to be satisfied is the law of conservation of momentum, the impulse balance. Based upon this law we formulate the equations of motion

$$L\sigma^e + g^e = \dot{p}^e \quad (1)$$

in which

L = differential operator, describing the equilibrium conditions

σ^e = stress vector

p^e = distributed body impulse vector

g^e = distributed body load vector

The dot means differentiation with respect to time.

Constitutive equations:

The second law to be satisfied are the constitutive equations, the material laws. The constitutive equations relate the stresses and the impulses to the strains and the velocities. We require

$$\begin{aligned} \sigma^e &= D^e \varepsilon^e \\ p^e &= R^e v^e \end{aligned} \quad (2)$$

in which

D^e = rigidity matrix

R^e = density matrix

ε^e = strain vector

v^e = velocities

The constitutive equations can be enhanced to the formulation of visco-elastic materials by addition of a strain velocity term following

$$\sigma^e = D_1^e \varepsilon^e + D_2^e \dot{\varepsilon}^e \quad (2a)$$

In this way we introduce material damping into the properties.

Kinematic conditions:

Finally we have to satisfy the kinematic conditions formulated by

$$\begin{aligned} \varepsilon^e &= L^* u_c^e \\ v^e &= \dot{u}_c^e \end{aligned} \quad (3)$$

in which

L^* = differential operator, here the selfadjoint of L

u_c = displacements

The conditions (1) until (3) have to be satisfied everywhere within a domain Ω , say an element, limited by time and geometry.

Dynamic boundary conditions:

At the boundaries we have to satisfy the law of conservation of momentum, thus the impulse balance. We formulate the impulse balance by the condition:

$$-\sigma_n^e dA dt - p_n^e dV + P_n^e dS = 0 \quad (4)$$

in which

σ_n^e = resulting stresses at geometrical boundary A

p_n^e = body impulses, directions following tangent coordinates of A

P_n^e = distributed impulse at boundary S , defined by time and geometry

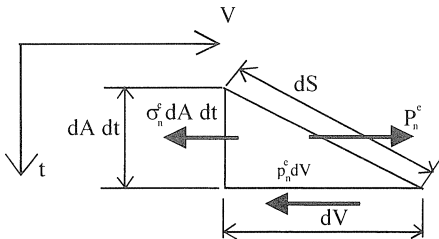


Fig. 1. Boundary of a time space element.

Mostly we will confine ourselves to pure geometrical boundaries, $dS = dAdt$ and to boundaries at fixed time points, $dS = dV$. Assuming the pure geometrical boundary then P_n^e equals to the traction force t_n^e , thus according to (4):

$$t_n^e - \sigma_n^e = 0 \quad (4a)$$

Assuming the boundary at a fixed time point then we get the boundary conditions

$$\begin{aligned} \pi_0^e &= p^e \text{ at } t = t_0 \\ \pi_1^e &= -p^e \text{ at } t = t_1 = t_0 + \Delta t \end{aligned} \quad (4b)$$

where

$$\begin{aligned} \pi_0^e &= \text{applied impulse at the beginning of time interval } \Delta t \\ \pi_1^e &= \text{"applied" impulse at the end of time interval } \Delta t \end{aligned}$$

Kinematic boundary conditions:

Both with respect to geometry and time we require compatibility of the displacements. At the boundaries we require

$$u_c^e = u_c^s \quad (5)$$

where

$$u_c^s = \text{displacements at boundary } S.$$

Assembly conditions:

During the assembly of the elements we will require the satisfaction of the impulse balance. In reference to (4) we require

$$\Sigma P_n^e = P_n^s \quad (6)$$

where P_n^s represents the applied impulse at boundary S .

Confining ourselves to the pure geometrical boundaries we get the equilibrium condition

$$\Sigma t_n^e = t_n^s \quad (6a)$$

in which t_n^s is the applied load at boundary A .

Confining ourselves to the boundaries at fixed time points we get the condition:

$$\pi_i^- + \pi_i^+ = \pi_i^t \quad (6b)$$

where

π_i^- = the impulse "applied" at the preceding time interval

π_i^+ = the impulse applied at the next time interval

π_i^t = the applied impulse at $t = t_i$

The Galerkin weak form

Limiting ourselves to the simple boundary conditions of (4a) and (4b) application of Galerkin's variational method to the conditions (1) until (5) yields the condition

$$\begin{aligned}
 R^e = & \int \int_{V^{\Delta t}} \delta \tilde{u}_c^T (L \tilde{\sigma}^e - \tilde{p}^e + g^e) dV dt + \oint_{A^{\Delta t}} \delta \tilde{u}_n^T (t_n^e - \tilde{\sigma}_n^e) dA dt + \\
 & + \int_{V^e} \delta \tilde{u}_c^T (\pi_0^e - \tilde{p}^e) |_{t=t_0} dV + \int_{V^e} \delta \tilde{u}_c^T (\pi_1^e + \tilde{p}_1^e) |_{t=t_1} dV = 0
 \end{aligned} \tag{7}$$

which should hold for every kinematically admissible variation δu_c^e of the continuous displacement field $\tilde{u}_c^e(x, y, z, t)$.

We will elaborate this condition. As a consequence of Green's lemma we can rewrite (7) as

$$\begin{aligned}
 R^e = & \int \int_{V^{\Delta t}} (-\delta \tilde{\varepsilon}^T \tilde{\sigma}^e + \delta \tilde{v}^T \tilde{p}^e + \delta \tilde{u}_c^T g^e) dV dt + \\
 & + \oint_{A^{\Delta t}} \delta \tilde{u}_n^T t_n^e dA dt + \int_{V^e} \delta \tilde{u}_c^T \pi_0^e dV + \int_{V^e} \delta \tilde{u}_c^T \pi_1^e dV = 0
 \end{aligned} \tag{8}$$

Applying the more general boundary condition of (4) we can write for (8):

$$R^e = \int_{\Omega^e} (-\delta \tilde{\varepsilon}^T \tilde{\sigma}^e + \delta \tilde{v}^T \tilde{p}^e + \delta \tilde{u}_c^T g^e) d\Omega + \oint \delta \tilde{u}_n^T P_n^e dS = 0 \tag{9}$$

Dropping the time boundary term we easily recognize Hamilton's variational principle.

Based upon (8) or (9) we can develop our finite element models.

Linear models

The basic choice is to take the approximations of the displacements that satisfy the kinematic conditions. The simplest way is to define a time interval Δt , with initial displacements u_0^e and final displacements u_1^e , and to approximate the displacements in between in a linear way following

$$u^e(t) = \alpha_0(t) u_0^e + \alpha_1(t) u_1^e \tag{10}$$

with

$$\alpha_0(t) = \frac{1}{2} - \frac{t}{\Delta t}$$

$$\alpha_1(t) = \frac{1}{2} + \frac{t}{\Delta t}$$

The time interval is illustrated in figure 2. A *conforming* displacement field in the time domain is achieved in this way.

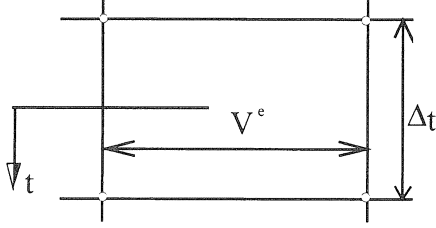


Fig. 2. A linear time space element.

Within the elements, between the geometrical boundaries, we take the classical shape functions following

$$\tilde{u}_c^e(x, y, z, t) = N^e(x, y, z)u^e(t) \quad (11)$$

with the time dependent nodal displacements $u^e(t)$.

Substitution of (10) and (11) into variational condition (8) yields a condition that is formulated with the use of the well known stiffness matrix K^e , damping matrix C^e and mass matrix M^e and consistent impulse vector m^e .

We obtain

$$R^e = -\delta u_0^{eT} H_{00}^e u_0^e - \delta u_0^{eT} H_{01}^e u_1^e - \delta u_1^{eT} H_{10}^e u_0^e - \delta u_1^{eT} H_{11}^e u_1^e + \delta u_0^{eT} m_0^{e+} + \delta u_1^{eT} m_1^{e-} = 0 \quad (12)$$

in which

$$H_{ij}^e = a_{ij} \Delta t K^e + b_{ij} C^e + c_{ij} \frac{1}{\Delta t} M^e \quad (13)$$

and

$$K^e = \int_{V^e} B^{eT} D_1 B^e dV \quad \text{stiffness matrix}$$

$$C^e = \int_{V^e} B^{eT} D_2 B^e dV \quad \text{damping matrix}$$

$$M^e = \int_{V^e} N^{eT} R N^e dV \quad \text{mass matrix}$$

in which B^e is the strain displacement matrix, relating the strains to the nodal displacements. For elaboration of the strain energy we can also apply a nonconforming displacement field, assuming

$$u^*(t) = \frac{1}{2}(u_0 + u_1) + \eta \frac{1}{\Delta t}(u_1 - u_0) \quad (14)$$

with free parameter η . Taking $\eta = 1$ yields the conforming model (10).

This parameter will be used to manipulate numerical stability and accuracy. Substitution hereof into (8) yields the coefficients of (13) following

$$a_{ij} = \begin{bmatrix} \frac{1}{4} + \frac{1}{12}\gamma & \frac{1}{4} - \frac{1}{12}\gamma \\ \frac{1}{4} - \frac{1}{12}\gamma & \frac{1}{4} + \frac{1}{12}\gamma \end{bmatrix} \quad b_{ij} = \begin{bmatrix} \frac{1}{2} & \frac{1}{2} \\ \frac{1}{2} & -\frac{1}{2} \end{bmatrix} \quad c_{ij} = \begin{bmatrix} -1 & 1 \\ 1 & -1 \end{bmatrix} \quad (15)$$

in which $\gamma = \eta^2$

We will obtain the same results by adding a contribution ΔG to the Galerkin residue following

$$\Delta G = \int_{\Delta t} \psi_2 \Delta t^2 \delta v^T K v dt \quad (16)$$

where $\psi_2 = \frac{1}{12}(\gamma - 1)$.

The vector m^e is called the consistent impulse vector, given by

$$\begin{bmatrix} m_0^{e+} \\ m_1^{e-} \end{bmatrix} = \int_{\Delta t} \begin{bmatrix} \alpha_0 \\ \alpha_1 \end{bmatrix} \int_{V^e} N^{eT} g^e dV dt + \int_{\Delta t} \begin{bmatrix} \alpha_0 \\ \alpha_1 \end{bmatrix} \int_{A^e} N_n^{eT} \mathbf{t}_n^e dA dt + \int_{V^e} N^{eT} \begin{bmatrix} \pi_0^e \\ \pi_1^e \end{bmatrix} dV \quad (17)$$

Since $R^e = 0$ for every kinematically admissible variation δu^e it should hold that

$$\begin{aligned} H_{00}^e u_0^e + H_{01}^e u_1^e &= m_0^{e+} \\ H_{10}^e u_0^e + H_{11}^e u_1^e &= m_1^{e-} \end{aligned}$$

For all elements together we have to comply with

$$\begin{aligned} H_{00} u_0 + H_{01} u_1 &= m_0^+ \\ H_{10} u_0 + H_{11} u_1 &= m_1^- \end{aligned} \quad (18)$$

The equations (18) can be interpreted as the relation between the discrete displacements u_0 and u_1 at the time points $t = t_0$ and $t = t_1$ and the equivalent impulse loads at the same time points. The correspondence with the static finite element method is striking. In the statics we relate lumped forces to discrete displacements, here we relate lumped impulses to discrete displacements.

In these equations the initial displacements u_0 and impulses m_0^+ are known whereas the displacements u_1 and impulses m_1^- are not known. From (18) we solve u_1 following

$$u_1 = H_{01}^{-1}(m_0^+ - H_{00}u_0)$$

and subsequently

$$m_1^- = H_{10}u_0 + H_{11}u_1$$

Together with the applied impulse load m_1^t at $t = t_1$ this consistent vector yields the initial impulses m_1^+ for the next time interval

$$m_1^- + m_1^+ = m_1^t$$

Because the most relevant applications of direct integration processes are found in the nonlinear problems, we will apply iteration schemes to the residual impulses. Given an estimate of the displacements $\tilde{u}(t)$ we calculate, using (8), the initial impulses. The residue that remains will be used to calculate an increment $\Delta\tilde{u}(t)$ to the displacements $\tilde{u}(t)$ – see figure 3 –. This process is repeated until sufficient accuracy is arrived.

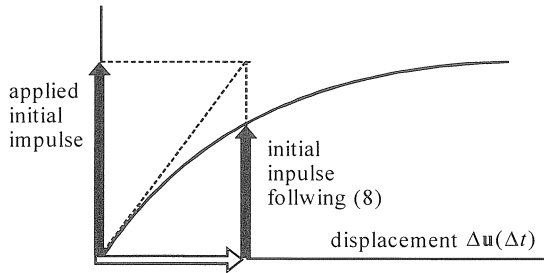


Fig. 3. An iteration procedure based upon residual impulses.

Quadratic models

The models discussed in the previous section have been based on a linear approximation with respect to time. These models possess $O[\Delta t]$ accuracy with respect to time. In order to obtain $O[\Delta t^2]$ accuracy we have to apply higher-order approximations with respect to time. For this purpose we introduce per time interval Δt^e midtime discrete value per degree of freedom (d.o.f).

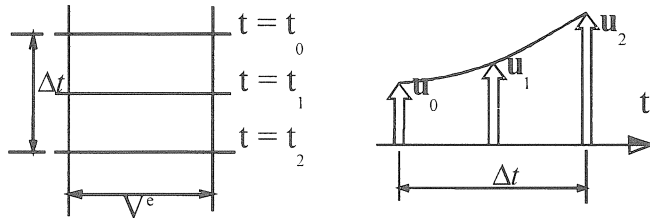


Fig. 4. Discrete values with respect to time.

Dropping superscript e we describe the displacement field by

$$\mathbf{u}(t) = \alpha_0(t)\mathbf{u}_0 + \alpha_1(t)\mathbf{u}_1 + \alpha_2(t)\mathbf{u}_2 \quad (19)$$

with

$$\alpha_0(t) = -\frac{1}{\Delta t} \left(1 - 2\frac{t}{\Delta t} \right)$$

$$\alpha_1(t) = 1 - 4\frac{t^2}{\Delta t^2}$$

$$\alpha_2(t) = \frac{t}{\Delta t} \left(1 + 2\frac{t}{\Delta t} \right)$$

Substitution into the variational condition (8) yields the matrices H_{ij} following

$$H_{ij} = a_{ij}\Delta t K + b_{ij}C + c_{ij}\frac{1}{\Delta t}M \quad (20)$$

Again we can take nonconforming modifications of the displacement field for the evaluation of the strain energy by assuming

$$\mathbf{u}^*(t) = \frac{1}{6}\mathbf{u}_0 + \frac{2}{3}\mathbf{u}_1 + \frac{1}{6}\mathbf{u}_2 + \frac{t}{\Delta t}(\mathbf{u}_2 - \mathbf{u}_0) - 2\eta \left(\frac{1}{12} - \frac{t^2}{\Delta t^2} \right) (\mathbf{u}_0 - 2\mathbf{u}_1 + \mathbf{u}_2) \quad (21)$$

with free parameter η .

Now we obtain the coefficients

$$a_{ij} = \begin{bmatrix} \frac{1}{9} + \frac{1}{45}\gamma & \frac{1}{9} - \frac{2}{45}\gamma & -\frac{1}{18} + \frac{1}{45}\gamma \\ \frac{1}{9} - \frac{2}{45}\gamma & \frac{4}{9} + \frac{4}{45}\gamma & \frac{1}{9} - \frac{2}{45}\gamma \\ -\frac{1}{18} + \frac{1}{45}\gamma & \frac{1}{9} - \frac{2}{45}\gamma & \frac{1}{9} + \frac{1}{45}\gamma \end{bmatrix} \quad b_{ij} = \begin{bmatrix} -\frac{1}{2} & \frac{2}{3} & -\frac{1}{6} \\ -\frac{2}{3} & 0 & \frac{2}{3} \\ \frac{1}{6} & -\frac{2}{3} & \frac{1}{2} \end{bmatrix} \quad c_{ij} = \begin{bmatrix} -\frac{7}{3} & \frac{8}{3} & -\frac{1}{3} \\ \frac{8}{3} & -\frac{16}{3} & \frac{8}{3} \\ -\frac{1}{3} & \frac{8}{3} & -\frac{7}{3} \end{bmatrix} \quad (22)$$

with $\gamma = \eta^2$.

We obtain the same results by addition of a contribution ΔG to the Galerkin residue following

$$\Delta G = \int_{\Delta t} \psi_4 \Delta t^4 \delta \mathbf{v}^\top K \mathbf{v} \, dt \quad (23)$$

with $\psi_4 = \frac{1}{45}(\gamma - 1)$

The resulting equations are given by

$$\begin{aligned} H_{00}u_0 + H_{01}u_1 + H_{02}u_2 &= m_0^+ \\ H_{10}u_0 + H_{11}u_1 + H_{12}u_2 &= m_1 \\ H_{20}u_0 + H_{21}u_1 + H_{22}u_2 &= m_2^- \end{aligned} \quad (24)$$

Here the initial displacements u_0 and the impulse vectors m_0^+ and m_1 are known, whereas displacements u_1 and u_2 and impulse vector m_2^- are unknown.

From (24) we solve the displacements u_1 and u_2 by

$$\begin{aligned} H_{01}u_1 + H_{02}u_2 &= m_0^+ - H_{00}u_0 \\ H_{11}u_1 + H_{12}u_2 &= m_1 - H_{10}u_0 \end{aligned}$$

and successively we compute the impulse vector by backsubstitution

$$m_2^- = H_{20}u_0 + H_{21}u_1 + H_{22}u_2$$

With m_2^- and applied impulse load m_2^+ we have the initial impulses for the next time interval.

Numerical stability, accuracy and damping

Numerical stability

Numerical unstable processes show an exponential growth of some contributions in the solution. Because of the exponential character of this erroneous contribution the process “crashes”. It turns out that this behavior is dependent on the choice of time step Δt .

To investigate these processes we develop an error $\Delta u_i = e_i$ at $t = i\Delta t$ into a series of vibration modes ϕ_k following

$$e_i = \sum_k \alpha_i^{(k)} \phi_k \quad (25)$$

with participation factors $\alpha_i^{(k)}$

We consider the development of e as a result of an initial displacement error Δu_0 and an initial impulse load error Δm_0^+ . No other loads are applied. Substitution of (25) into the equations of motion and application of the orthogonality relations

$$\phi_k^T \mathbf{K} \phi_m \begin{cases} = 0 & k \neq m \\ = \omega_k^2 & k = m \end{cases} \quad \phi_k^T \mathbf{C} \phi_m \begin{cases} = 0 \\ = 2\xi_k \omega_k \end{cases} \quad \phi_k^T \mathbf{M} \phi_m \begin{cases} = 0 & k \neq m \\ = 1 & k = m \end{cases} \quad (26)$$

yields, for each vibration mode, the equations of motion

$$h_{ij} \alpha_j \begin{cases} = \mu_0^+ & i = 0 \\ = 0 & i = 1, 2, \dots, n-1 \\ = \mu_n^- & i = n \end{cases} \quad (27)$$

with

$$\begin{aligned} h_{ij} &= \phi_k^T \mathbf{H}_{ij} \phi_k \\ \mu_0^+ &= \phi_k^T \mathbf{m}_0^+ \quad k = 1, 2, \dots \\ \mu_n^- &= \phi_k^T \mathbf{m}_n^- \end{aligned}$$

where $n = 1$ for the linear models and $n = 2$ for the quadratic models.

The solution of the uncoupled equations of motion is given by

$$\alpha_i = \lambda^i \alpha_0$$

Multiplication factor λ is called the spectral radius; if $|\lambda| > 1$ then the process is called numerically unstable, if $|\lambda| \leq 1$ then the process is called numerically stable.

Investigation of the spectral radius of the linear models shows numerical stability if

$$\gamma \omega^2 \Delta t^2 \leq 12 \tag{28}$$

Unconditional numerical stability is ensured if $\gamma \leq 0$.

Investigation of the spectral radius of the quadratic models shows unstable solutions if

$\omega^2 \Delta t^2 \in \left[\frac{60}{\gamma + 5}, 12 \right]$ and if $\omega^2 \Delta t^2 > \frac{60}{\gamma}$. Unconditional numerical stability is ensured only, and only if $\gamma = 0$.

Accuracy

The accuracy of a model is responsible for the convergence speed to the exact solution. For our models we can use an appropriate choice of γ to optimize the accuracy. To elaborate this process we need a reference criterion; we will use the so-called "action", given by the product of impulses and displacements. Per vibration mode we will investigate the resulting action

$$action = \alpha_0 \mu_0 + \alpha_n \mu_n$$

The exact solution of the uncoupled equations of motion is known.

Both for the linear models and the quadratic models $\gamma = 2$ yields extremely high accuracy. It has to be noted, however, that these models possess a limited numerical stability, while damping properties are ignored. Because of these restrictions the use of these models is but limited.

Numerical damping

The classic models, such as the Newmark- β method, ignore physical damping with growing Δt

Investigation of the spectral radius of unconditional numerical stable processes with nonzero physical damping shows that $|\lambda| \rightarrow 1$ for $\omega \Delta t \rightarrow \infty$.

The effect of physical damping, especially of the high frequency modes, is negligible. Consequently disturbances caused by high frequency modes can be a source of inaccuracies.

In order to maintain damping properties for large values of $\omega \Delta t$ we introduce numerical damping, which is proportional to the stiffness matrix K . We add damping to our models by the addition of a contribution ΔG to the Galerkin variational condition following

where

$$C = \psi_1 \Delta t K$$

Taking the damping coefficients dependent on the time step Δt the damping contribution does not vanish for large values of $\omega \Delta t$. Physically this is meaningless; it is purely a numerical tool to improve the properties of the numerical process. We call this contribution numerical damping. Together with (16) we can manipulate the properties of the linear models by the addition ΔG to the Galerkin variational condition of the compatible model following

$$\Delta G = \int_{\Delta t} (\psi_1 \Delta t \delta u^T K v + \psi_2 \Delta t^2 \delta v^T K v) dt \quad (29)$$

In the same way we can manipulate the properties of the quadratic model by addition of the contribution

$$\Delta G = \int_{\Delta t} (\psi_1 \Delta t \delta u^T K v + \psi_2 \Delta t^2 \delta v^T K v + \psi_3 \Delta t^3 \delta v^T K \dot{v} + \psi_4 \Delta t^4 \delta \dot{v}^T K \dot{v}) dt \quad (30)$$

Investigation of the spectral radius of the linear models shows that numerical damping is most efficient for

$$\begin{aligned} \psi_1^2 &= \frac{1}{3} \gamma \\ \psi_2 &= \frac{1}{12} (\gamma - 1) < -\frac{1}{12} \end{aligned} \quad (31)$$

The coefficients a_{ij} are given by

$$a_{ij} = \begin{bmatrix} \frac{1}{3} - \frac{1}{2} \psi_1 + \psi_2 & \frac{1}{6} + \frac{1}{2} \psi_1 - \psi_2 \\ \frac{1}{6} - \frac{1}{2} \psi_1 - \psi_2 & \frac{1}{3} + \frac{1}{2} \psi_1 + \psi_2 \end{bmatrix} \quad (32)$$

Coefficients b_{ij} and c_{ij} do not change.

Figure 5 shows the spectral radius of a physically damped system ($\zeta \neq 0$) with and without numerical damping.

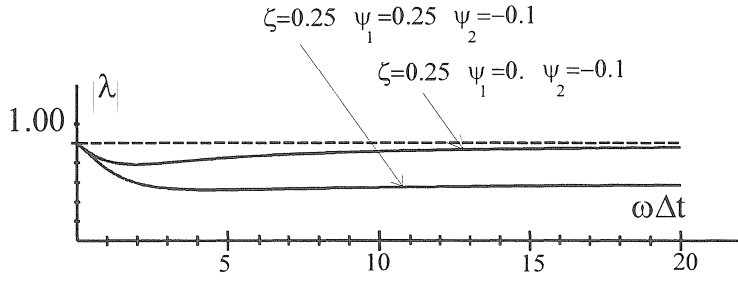


Fig. 5. Spectral radius linear models.

Investigation of the spectral radius of the quadratic models shows that numerical damping is possible if

$$\begin{aligned}
 \psi_1 &= 0 \\
 \psi_2 > 0, \psi_3 > 0 \\
 \psi_4 &= \frac{1}{45}(\gamma - 1) = -\frac{1}{45}
 \end{aligned} \tag{33}$$

Coefficients a_{ij} are now given by

$$a_{ij} = \begin{bmatrix} \frac{1}{9} - \frac{7}{3}\psi_2 - 4\psi_3 & \frac{1}{9} + \frac{8}{3}\psi_2 + 8\psi_3 & -\frac{1}{18} - \frac{1}{3}\psi_2 - 4\psi_3 \\ \frac{1}{9} + \frac{8}{3}\psi_2 & \frac{4}{9} - \frac{16}{3}\psi_2 & \frac{1}{9} + \frac{8}{3}\psi_2 \\ -\frac{1}{18} - \frac{1}{3}\psi_2 + 4\psi_3 & \frac{1}{9} + \frac{8}{3}\psi_2 - 8\psi_3 & \frac{1}{9} - \frac{7}{3}\psi_2 + 4\psi_3 \end{bmatrix} \tag{34}$$

The coefficients b_{ij} and c_{ij} do not change.

Figure 6 shows the spectral radius of a model with and a model without numerical damping.

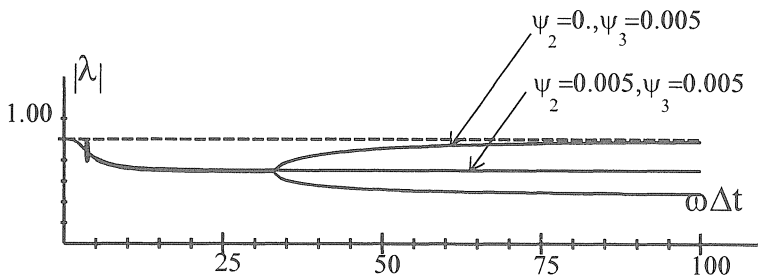


Fig. 6. Spectral radius of quadratic models

This model is expected to be both accurate and robust; much experience, however, is not yet available.

Numerical simulation of a track train interaction

To demonstrate the advantage of modelling to time and geometry in the same step we show a model for the analysis of the interaction of a moving vehicle (a train) and the supporting structure (the track and foundation). We consider four wheels of the train moving with a constant speed v ; only vertical forces are considered – see figure 7 –.

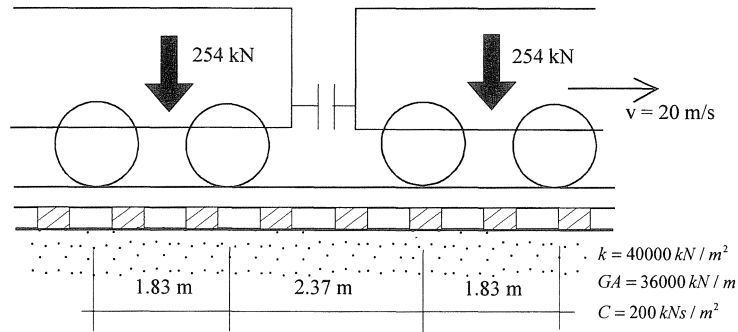


Fig. 7. A moving train on a rail track.

Each of the structure components contributes to the stiffness, damping and/or inertia properties of the problem. We will consider each of them separate.

Moving vehicle:

Based upon experiments Cox showed that a moving vehicle can be modeled by independent moving two mass spring systems – see figure 8 –. Each wheel is represented by three moving d.o.f's.

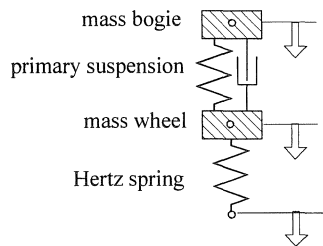


Fig. 8. Model of a moving wheel.

Rail:

The rail is modeled by Timoshenko beams, taking into account bending, shear deformation, translational inertia and rotational inertia.

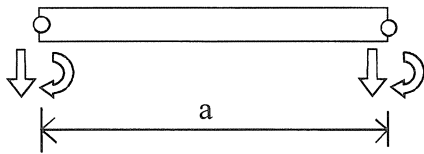


Fig. 9. Rail element.

Sleeper and rail pad:

Maree showed the role of rail pad contribution to stiffness and damping properties. The stiffness and damping are smeared out about a four-node element with the width of the sleeper – see figure 10 –. The sleeper cross section is assumed to be rigid; only the mass properties are taken into account.

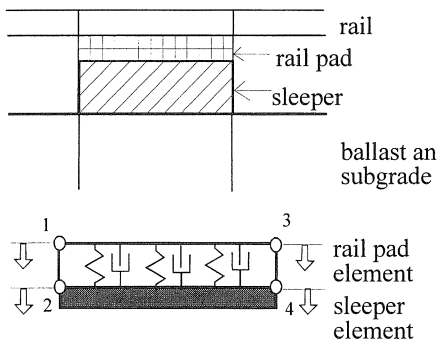


Fig. 10. Model of the rail pad and sleeper.

Contact sleeper ballast:

It is assumed that the contact face between sleeper and ballast is unbonded, which means that no tension forces between sleeper and ballast are possible. We model this contact by a gap element between sleeper and ballast

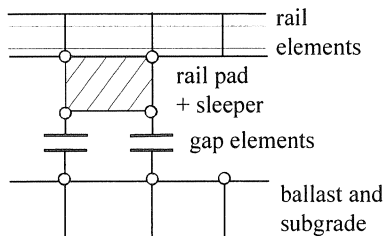


Fig. 11. Modelling the contact face between sleeper and ballast.

Ballast and subgrade:

Vertical direct stresses and shear stresses (Pasternak foundation) contribute to deformation of ballast and subgrade, inertia is modeled by some mass contribution and damping by viscoelastic dampers. The shear stiffness is modeled by a shear layer, the mass is added to this shear layer. The vertical direct stresses are modeled by distributed Winkler springs while viscoelastic dampers are added in the same way. A two-node element models all these contributions – see figure 12 –.

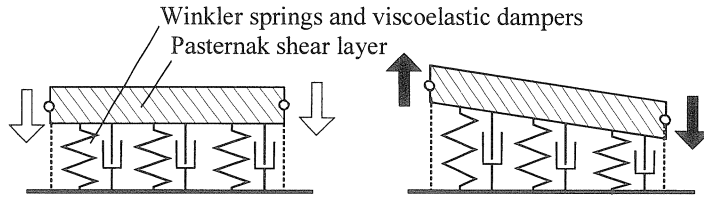


Fig. 12. Model of ballast and subgrade.

Silent boundaries:

The function of a silent boundary is to model the surroundings of the f.e.m. model in such a way that all stress waves arriving at the boundary do not reflect. The ideal silent boundary will pass any stress wave contribution into the surroundings

It turns out that the silent boundary condition can be modeled by visco-elastic dampers with a damping factor $c_s = \sqrt{G\rho}A$ for the shear forces and $c_\phi = \sqrt{E\rho}I$ for the bending moments.

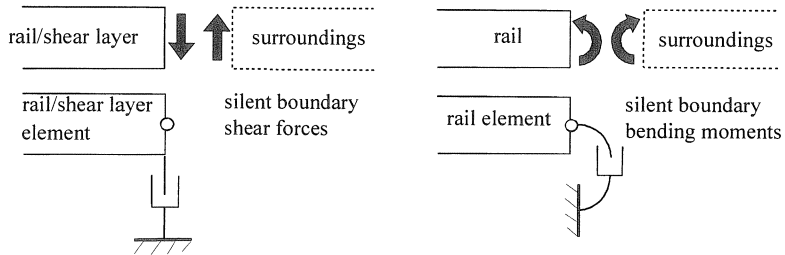


Fig. 13. Silent boundaries.

The model of a moving vehicle introduces some d.o.f's which move with respect to the supporting track structure.

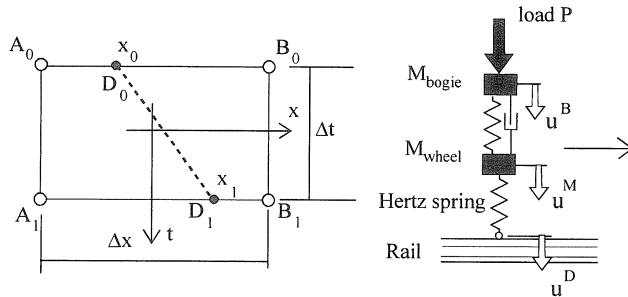


Fig. 14. Moving vehicle crossing a time space element.

To introduce a moving vehicle into the track system we have to couple the degree of freedom u^D – see figure 14 – to the rail d.o.f.'s. We will assume that

$$\begin{aligned} u_0^D &= \left(\frac{1}{2} - \xi_0\right)u_0^A + \left(\frac{1}{2} + \xi_0\right)u_0^B \\ u_1^D &= \left(\frac{1}{2} - \xi_1\right)u_1^A + \left(\frac{1}{2} + \xi_1\right)u_1^B \end{aligned} \quad (35)$$

where $\xi_0 = \frac{x_0}{\Delta x}$ and $\xi_1 = \frac{x_1}{\Delta x}$.

Introducing

$$\mathbf{u}^{\text{veh}} = \begin{bmatrix} u^B \\ u^M \\ u^D \end{bmatrix}$$

we formulate the coupling condition by

$$\begin{aligned} \mathbf{u}_0^{\text{veh}} &= \mathbf{T}_0 \mathbf{u}_0 \\ \mathbf{u}_1^{\text{veh}} &= \mathbf{T}_1 \mathbf{u}_1 \end{aligned} \quad (36)$$

The vehicle's contribution to the Galerkin's condition is given by

$$R_{\text{veh}} = \delta \mathbf{u}^{\text{veh}\top} \mathbf{H}^{\text{veh}} \mathbf{u}^{\text{veh}} - \delta \mathbf{u}^{\text{veh}\top} \mathbf{p}^{\text{veh}}$$

that results into the equations of motion

Substitution of the coupling condition (36) yields

$$\begin{bmatrix} \mathbf{T}_0^\top \mathbf{H}_{00}^{\text{veh}} \mathbf{T}_0 & \mathbf{T}_0^\top \mathbf{H}_{01}^{\text{veh}} \mathbf{T}_1 \\ \mathbf{T}_1^\top \mathbf{H}_{10}^{\text{veh}} \mathbf{T}_0 & \mathbf{T}_1^\top \mathbf{H}_{11}^{\text{veh}} \mathbf{T}_1 \end{bmatrix} \begin{bmatrix} \mathbf{u}_0 \\ \mathbf{u}_1 \end{bmatrix} = \begin{bmatrix} \mathbf{T}_0^\top \mathbf{f}_0^{\text{veh}} \\ \mathbf{T}_1^\top \mathbf{f}_1^{\text{veh}} \end{bmatrix} \quad (37)$$

or

$$\begin{aligned} \mathbf{H}_{00}^* \mathbf{u}_0 + \mathbf{H}_{01}^* \mathbf{u}_1 &= \mathbf{p}_0^* \\ \mathbf{H}_{10}^* \mathbf{u}_0 + \mathbf{H}_{11}^* \mathbf{u}_1 &= \mathbf{p}_1^* \end{aligned} \quad (38)$$

It has to be noted that matrix \mathbf{H}_{01}^* is no more symmetric.

In structures such as a rail track the stiffness properties of the materials vary strongly. Especially the rail (steel) is very stiff with respect to the subgrade. Because of the large stiffness variations the physical damping of the stiff parts is, usually, simulated inadequately by the numerical process

which results into overshoot as shown in figure 15. This poor behaviour can be improved by the addition of numerical damping to the model following

$$C = \psi_1 \Delta t K \quad (39)$$

The maximum numerical damping – see (31) – is obtained by the substitution of $\psi_1 = \sqrt{\frac{1}{3}}\gamma$.

The strongest damping (superdamping) is obtained with $\gamma = -3$. It is recommended to use this value for the addition of numerical damping to the rail elements; for all other elements we take $\gamma = -0.1$.

In figure 15 the shear force in a rail element is shown using $\gamma = -0.1$ and $\gamma = -3$.

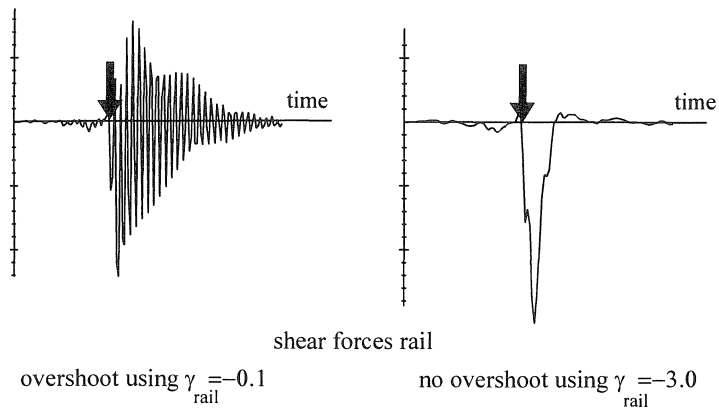


Fig. 15.

This model has been applied to simulate the wheel track interaction at some parts of the South African coal line. Some of the most significant parameters are

spacing sleepers	0.65 m
wheel loads	$P = 120 \text{ kN}$
subgrade modulus	$k = 40000 \text{ kN/m}^2$
shear layer	$GA = 36000 \text{ kN/m}$
rail profile	R-60 (South African rail profile)

Results are shown for the displacements, the bending moments and the rail pad forces.

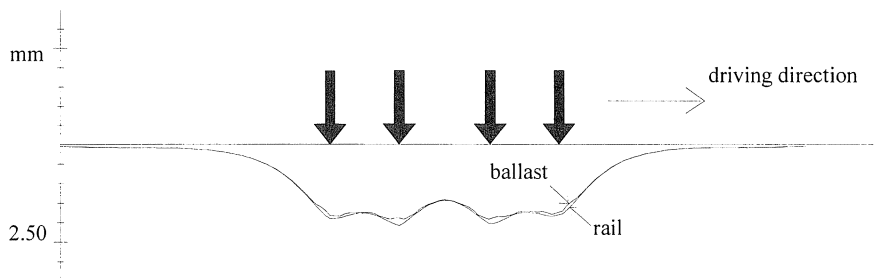


Fig. 16. Displacements at $t = 0.66$.

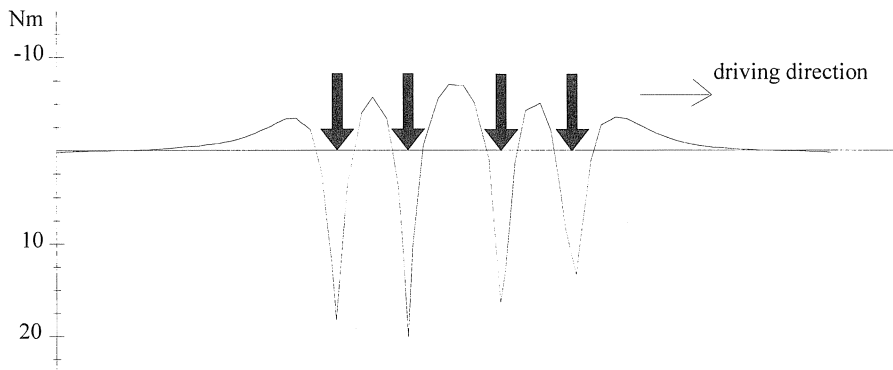


Fig. 17. Bending moments at $t = 0.66$.

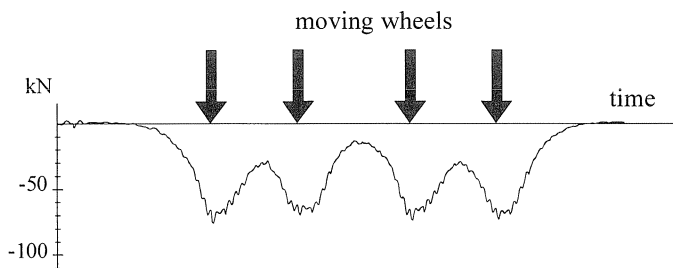


Fig. 18. Rail pad forces.

Conclusions

Based upon a concise formulation with respect to time and geometry of the governing equations numerical models are developed which relate lumped impulses to discrete displacements. These models are presented as single step procedures, thus easy to interrupt and to restart. No continuity of velocities and accelerations are required; only the physical request of lumped impulse balance and continuity of the displacements is satisfied.

A robust direct integration method requires unconditional numerical stability and effective numerical damping. The introduction of nonconforming elements provides the flexibility to manipulate the properties with respect to numerical stability, accuracy and damping.

Both for the linear and the quadratic models a class of unconditionally numerical stable and effectively damping models can be selected.

The application to simulate the wheel track interaction shows the natural way to model unusual structural problems such as moving d.o.f's as well to solve local overshoot problems.

References

- BATHE, K.J. , WILSON, E.L., (1976), "Numerical methods in finite element analysis", Prentice Hall, Englewood Cliffs, N.J.
- BAZZI, G., ANDERHEGGEN, E. (1982), "The r-family of algorithms for timestepintegration with improved numerical dissipation", *Earthquake Eng. and Struct. Dyn.*, **10**, p. 765-771.
- BLAAUWENDRAAD, J. KOK, A.W.M. (1987), "Handicraft in finite elements", *Proc. Int. Conf. Num. Meth. Engng*, Swansea, NUEMETA 87.
- COX, S.J., (1985), "Test on railway vehicle characteristics", Pandrol Report No 1074, London.
- FREDERIC, C.O. (1981), "The effect of rail straightness on track maintenance", Procs Conf. on Advanced Techniques in Permanent Way Design, Construction and Maintenance, Madrid.
- GRASSIE, S.L. (1984), 'Dynamic modelling of railway track and wheelsets', Procs 2-nd Int.. Conf. Recent Advances Struct. Dyn., University of Southampton.
- HILBER, H.B., Hughes, Th.J.R. (1978), "Collocation, dissipation and "overshoot" for time integration schemes in structural dynamics", *Earthquake Eng. and Struct. Dyn.*, **6**, p. 99-117.
- HILBER, H.M., HUGHES, TH.J.R., TAYLOR, R.L. (1977), "Improved numerical dissipation for time integration algorithms in structural dynamics", *Earthquake Eng. and Struct. Dyn.*, **5**, p. 283-292.
- HUGHES, Th.J.R. (1987), "The finite element method", Prentice Hall, Englewood Cliffs, N.J.
- HUGHES, Th.J.R. (1983), "Transient algorithms and stability", in "Computational methods for transient analysis", p. 67-155, Elseviers, Amst.
- KLEIN, S., TRUJILLO, D.M., "An unconditionally stable finite element analysis for nonlinear structures", *Comp. & Struct.*, 1983, **16**, p. 187-197.
- KOK, A.W.M. (1981), "A theoretical manual for STRUDL", JRC Euratom, Ispra
- KOK, A.W.M. (1995), "Lumped pulses and discrete displacements", Doct. thesis, Delft University of Technology, Delft.
- KOK, A.W.M. (1981), "Pulses in finite elements", *Proc. First. Conf. on Comp. in Civ. Engng.*, N.Y
- KRIEG, R.D. (1973), "Unconditional stability in numerical time integration methods", *J. Appl. Mech.*, **40**, p. 417-421.
- MAREE, J.S. (1993), "Dynamic behaviour of track with resilient railpads", Thesis report, University of Pretoria, Pretoria.
- NEWMARK, N.M.(1959), "A method of computation for structural dynamics", *J. Engng Div., ASCE*, **85**, p. 67-94.
- WOOD, W.L., BOSSAK, M., ZIENKIEWICZ, O.C. (1980), "An alpha modification of Newmark's method", *Int. J. Num. Meth. Eng.*, **15**, p. 1562-1566.

ZIENKIEWICZ, O.C., WOOD, W.L. HINE, N.W., Taylor, R.L.(1984), "A unified set of single step algorithms, Part 1: General formulation and applications," *Int. J.Num. Meth. in Engng.*, **20**, p. 1529-1552.

ZIENKIEWICZ, O.C., 'A new look at the Newmark, Houbolt and other time stepping formulae: a weighted residual approach', *Earthq. Engng. Struc.Dyn.*, 1977, **5**, p. 413-418,1977.